



**HAL**  
open science

## Co-promoted Mo-carbide catalytic system for sustainable manufacturing of chemicals via co-processing of CO<sub>2</sub> with ethane

Vera Bikbaeva, Nikolay Nesterenko, Nuria García-Moncada, Valentin Valtchev

### ► To cite this version:

Vera Bikbaeva, Nikolay Nesterenko, Nuria García-Moncada, Valentin Valtchev. Co-promoted Mo-carbide catalytic system for sustainable manufacturing of chemicals via co-processing of CO<sub>2</sub> with ethane. *Green Carbon*, 2023, 1 (1), pp.94-103. 10.1016/j.greenca.2023.09.001 . hal-04270588

**HAL Id: hal-04270588**

**<https://hal.science/hal-04270588>**

Submitted on 4 Nov 2023

**HAL** is a multi-disciplinary open access archive for the deposit and dissemination of scientific research documents, whether they are published or not. The documents may come from teaching and research institutions in France or abroad, or from public or private research centers.

L'archive ouverte pluridisciplinaire **HAL**, est destinée au dépôt et à la diffusion de documents scientifiques de niveau recherche, publiés ou non, émanant des établissements d'enseignement et de recherche français ou étrangers, des laboratoires publics ou privés.

# Co-promoted Mo-carbide catalytic system for sustainable manufacturing of chemicals via co-processing of CO<sub>2</sub> with ethane

Vera Bikbaeva<sup>a</sup>, Nikolay Nesterenko<sup>a,\*</sup>, Nuria García-Moncada<sup>b</sup> and Valentin Valtchev<sup>a</sup>

<sup>a</sup> Laboratoire Catalyse et Spectrochimie, ENSICAEN, Université de Caen, CNRS, 6 Boulevard Maréchal Juin, 14050 Caen, France; valentin.valtchev@ensicaen.fr

<sup>b</sup> Servicios Generales de Investigación, XPS, Centro de Investigación, Tecnología e Innovación de la Universidad de Sevilla (CI-TIUS), Av. Reina Mercedes 4B, 41012, Sevilla, Spain; ngarcia2@us.es

\* Corresponding author. E-mail: nikolay.nesterenko@sulzer.com (NN)

ORCID. Vera Bikbaeva: 0000-0002-5946-3814

Nikolay Nesterenko: 0000-0002-8936-3275

Nuria García-Moncada: 0000-0003-0218-1135

Valentin Valtchev: 0000-0002-2341-6397

Received: Day Month Year; Accepted: Day Month Year; Available online: Day Month Year

---

**ABSTRACT:** The study reports progress in developing a molybdenum carbide-based catalyst for co-processing ethane and CO<sub>2</sub>. The cobalt promoting of molybdenum carbide improved the activity and stability of ethane transformation in the presence of CO<sub>2</sub> substantially without any impact on ethylene selectivity. The Mo-Co supported catalyst also showed interesting performance in catalyzing ethane dry reforming and that application could be a perspective further use for this system. In addition, the comprehensive analysis of mono- and bi-metallic catalysts revealed that Co-promoting prevented rapid Mo-carbide oxidation. Further, tuning operation conditions allowed to control catalyst's selectivity and maximize CO<sub>2</sub> utilization or ethylene formation.

**Keywords:** CO<sub>2</sub> utilization; oxidative dehydrogenation; CO<sub>2</sub> negative ethylene production; cobalt-molybdenum synergy; embryonic zeolite.

© 2023 The Authors. Production and hosting by Elsevier B.V. This is an open access article under the CC BY-NC-ND license (<http://creativecommons.org/licenses/by-nc-nd/4.0/>).

---

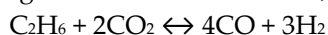
## 1. Introduction

Amid the climate crisis reaching net-zero emissions of greenhouse gases by mid-century requires developing a solution for CO<sub>2</sub> circularity and designing low-carbon routes for olefins production [1]. Olefins are rapidly becoming the largest driver of global oil consumption. They will account for a third of the oil demand by 2030 and nearly half by 2050 [2]. Therefore, developing the low-carbon route for olefins production is an issue of high priority [1]. Besides, hydrogen is an important by-product of olefins production, but it is often not properly valorized due to high purification costs.

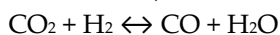
Global energy-related carbon dioxide emissions rose 6% in 2021, i.e., to 36.3 billion tonnes, their highest ever level, as the world economy rebounded strongly from the Covid-19 crisis [3]. The overall production of ethylene is about 220 million tons in 2022 [4], which offers a significant opportunity for CO<sub>2</sub> utilization while co-producing ethylene via reactions:



Direct non-catalytic Dehydrogenation of Ethane - DDE,  $\Delta H_{298\text{K}} = 137 \text{ kJ/mol}$ , Eq. (1),

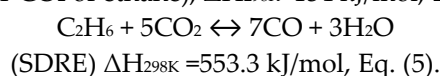
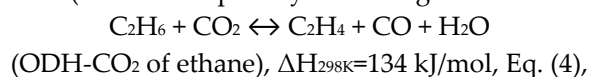


Dry Reforming of Ethane - DRE,  $\Delta H_{298\text{K}} = 428.1 \text{ kJ/mol}$ , Eq. (2),



Reverse Water Gas Shift – RWGS,  $\Delta H_{298\text{K}} = 41.2 \text{ kJ mol}$ , Eq. (3).

A combination of the above reactions results either in maximum ethylene production mode (so-called ODH-CO<sub>2</sub> of ethane) or in maximum CO<sub>2</sub> utilization (so-called super dry reforming of ethane - SDRE):



One can see that one mole of ethane transforms 5 moles of CO<sub>2</sub> to 7 moles of CO in the super dry reforming, which is an efficient way for CO<sub>2</sub> utilization. Noteworthy, both reactions (equations 4 and 5), occur at a relatively moderate temperature range allowing mitigation of coke formation. In contrast to the steam cracking of ethane, both routes are not very demanding for feedstock purity. They could be operated with a significant amount of ethylene, CO, C<sub>3+</sub> hydrocarbons, methane, and H<sub>2</sub> in the stream. The latter are typically present in off-gases of a refinery (including fluid catalytic cracking (FCC), hydrocracker, or delayed coker) or natural gas liquids (NGL). The abundance of these feedstocks opens an interesting perspective for using native CO<sub>2</sub> at the natural gas production sites and CO<sub>2</sub> circularity in a refinery.

Hence, the objective of the present work is *in situ* hydrogen utilization, which is co-produced with chemicals to convert CO<sub>2</sub> to CO (RWGS reaction) while maintaining ethylene production at the necessary level from opportunistic feedstocks. Consequently, the produced CO could be easily converted with green hydrogen to sustainable products via Fischer-Tropsch or MeOH intermediates. Based on equation 4, the process could reduce by 1% the overall amount of CO<sub>2</sub> emitted in 2021, considering the worldwide volume of ethylene production. Moreover, the CO<sub>2</sub> emissions could be further reduced if the process is operated close to DRE or SDRE conditions (equations 2 and 5, respectively).

The results for ODH-CO<sub>2</sub> of ethane resulted in 108% CO<sub>2</sub> reduction *vs.* conventional ethane cracking [5,6]. However, the existing catalytic system needs to be better understood and improved. Moreover, the CO<sub>2</sub> conversion during this process is the RWGS reaction accompanying the ethane dehydrogenation.

The utilization of CO<sub>2</sub> for the synthesis of high-valuable chemicals in syngas routes is gaining momentum [7]. This is an important brick in carbon circularity and is applied to synthesize many chemical products, for example, methanol, ethanol [8], olefins [9,10], dimethyl ether [11], or sustainable fuels. The CO<sub>2</sub> is typically reacted with hydrogen (in a separate or direct process) to a CO<sub>2</sub> – rich syngas stream, which is further reacted over a catalyst to produce the target product. One can see that the co-processing with ethane significantly reduces the on-purpose hydrogen consumption for CO<sub>2</sub> conversion to the product by performing *in situ* RWGS reaction with the production of CO [5,6,12-14].

The Reverse Water Gas Shift (RWGS) reaction is equilibrium-limited (equation 3) [15], and it works in the same range as ethane cracking: >600 °C. At lower temperatures, CO<sub>2</sub> conversion with H<sub>2</sub> tends to the methanation route [15].

RWGS occurs in the following catalytic systems: Cu-based metal oxide [16], supported Pt [17,18], Ru [19], Ni [20,21], Ni-Mo [22], and Mo [23-25] catalytic systems. The Mo-based systems are active in the reaction in the form of carbides. For CO<sub>2</sub> conversion with pure H<sub>2</sub> (RWGS), Mo<sub>2</sub>C activity depends on catalyst particle size [25]. Thus, a decrease in Mo<sub>2</sub>C cluster size to 0.5 nm improved both reaction rate and selectivity to CO. **Over the 0.5 nm carbide clusters**, the CO selectivity reached 99.6% when it was only 89% on bulky Mo<sub>2</sub>C. CO<sub>2</sub> conversion was measured from 30-55% at 600 °C. The formation of MoO<sub>2</sub> species was observed on the spent catalysts. Pajares et al. also demonstrated the partial formation of the MoO<sub>2</sub> phase during RWGS [26]. However, for the RWGS reaction, the carbide oxidation was not always observed [27]. In general, the MoO<sub>2</sub> formation starts to occur during the CO<sub>2</sub> reduction to CO by H<sub>2</sub> above 580 °C [28]. Therefore, the interest in such a system is rather limited due to its oxidation by CO<sub>2</sub> to the oxide form, which becomes critical for carbide-based catalysts applied under more harsh conditions: ODH-CO<sub>2</sub> of alkanes [29,30], and dry reforming of methane [31].

On the other side, MoO<sub>2</sub> could be carburized to Mo<sub>2</sub>C in a reaction with hydrocarbons [32,33]. The description of the oxidation-carburization cycle for the Mo<sub>2</sub>C-catalyst is given in the reference [34]. As mentioned, the Mo<sub>2</sub>C oxidation could be partially mitigated by the hydrocarbon environment, which opens opportunities to prevent full oxidation of the active phase leading to the activity decrease.

Molybdenum carbide has similar electronic characteristics to noble metals, which makes it potentially an attractive catalytic system [35]. During the multistep ethane and CO<sub>2</sub> conversion, its surface undergoes several changes. For instance, the Mo<sub>2</sub>C surface changes during the ODH-CO<sub>2</sub> reaction and their effect on the catalytic performance were reported [30]. A formation of the C-rich surface results in extra low ethane conversion.

For carbide catalyst design, preventing fast carbon accumulation on the active sites is a key task. An increase in the O-rich surface, e.g., the interaction with CO<sub>2</sub> allows more selective ethylene production. However, this leads to a de-

crease in the ethane conversion. In other words, the O-modification prevents a C-C scission, favoring the DRE pathway [36]. Hence, it could be deduced that under standard flow-bed reactor conditions, the equilibrium between various surface states with the prevention of full oxidation is a way to create the conditions for stable catalyst performance and high selectivity to the desired product.

One of the first reports on the Mo<sub>2</sub>C application for ODH-CO<sub>2</sub> reaction was published 1999 by Solymosi and Nemeth [37]. Ethylene selectivity from ethane was more than 95% at 9% ethane conversion at 580 °C (C<sub>2</sub>H<sub>6</sub>/CO<sub>2</sub>=1/2.7 vol/vol). Under an equimolar C<sub>2</sub>H<sub>6</sub>/CO<sub>2</sub> ratio, ethylene selectivity rose to 90% at 600 °C [37]. However, the reoxidation conversion Mo<sub>2</sub>C phase to oxy-carbides or oxides was the roadblock preventing further development of the catalyst.

Some advances in Mo<sub>2</sub>C stability were reported by Marquart et al. [29]. Their approach was based on a variation of the catalyst support, but still, the formation of MoO<sub>2</sub> via carbide oxidation was significant. Hydrogen addition to the feed resulted in a significant formation of CO over Mo<sub>2</sub>C/ZrO<sub>2</sub> and Mo<sub>2</sub>C/SiO<sub>2</sub> catalytic systems. With 17 vol.% H<sub>2</sub> in ethane and the equal ethane/CO<sub>2</sub> molar ratio, the observed conversion was about 7-8% with the maximal selectivity to ethylene of 75% at 600 °C. The conversion of CO<sub>2</sub> was about 40%. On the contrary, a very fast deactivation was observed without H<sub>2</sub> dilution of CO<sub>2</sub>.

Thus, the reoxidation of the Mo<sub>2</sub>C phase with CO<sub>2</sub> to oxycarbides or oxides during high-temperature processes remains the bottleneck for the utilization of this catalytic system and limits its activity in ODH-CO<sub>2</sub>. An alternative to solve this problem is to promote a supported Mo<sub>2</sub>C system by Co-addition. The addition of Co brings a soft hydrogenation function that is expected to prevent the reduction of the Mo-containing phase and is known for its synergetic effect in other applications such as hydrodesulfurization [38] and hydrocracking [39].

Co-promoted Mo sulfide catalytic systems are also effective for nitroarenes hydrogenation under lower pressure [40], while Co-Mo-P catalysts are applied for hydrodesulfurization [41]. The dehydrogenation properties of Co-based catalysts were demonstrated in many cases. For instance, isobutane dehydrogenation on supported cobalt catalyst was reported [42]. Cobalt single-atom catalyst for HCOOH dehydrogenation to CO and H<sub>2</sub> [43], and Co-MOR for the ethane dehydrogenation [44]. Also, Co-Mo systems (Co-Mo/Al<sub>2</sub>O<sub>3</sub>) showed improved methane conversion and catalyst stability in dry methane reforming [45]. Cobalt oxide for processing ethane with CO<sub>2</sub> led to an ethane dry reforming route [46].

Mo and Co carbide systems are also used as a catalyst for CO<sub>2</sub> processing. Hydrogenation properties of Co could be illustrated in RWGS. Co-promoted carbide Mo<sub>2</sub>C was applied for RWGS by Porosoff [47]. The CO:CH<sub>4</sub> product ratio was 51.3. Cobalt carbide was used as a catalyst for effective ethanol dehydrogenation with acetaldehyde production [48]. The carbide phase formation was achieved under steam reforming conditions at 500 °C.

This contribution reports the promotion effect of Co-promoting to the Mo<sub>2</sub>C catalyst. The catalyst was supported on embryonic zeolites, which proved to be an excellent carrier for a similar catalytic system [5]. The objective is to improve the activity by the Co addition without impacting the ethylene production. One of the goals of the study is to identify conditions that favor the ODH-CO<sub>2</sub> or DRE pathway. Also, a comprehensive study of the Co-promoting effect on the nature of the active phase, general catalyst stability, and oxidative resistance is an integral part of the present study.

## 2. Experimental section

### 2.1. Preparation of EZ carriers

Al-free embryonic zeolites (EZ<sub>Si</sub>) samples were prepared and used as a support for preparation of metal-containing catalyst by incipient wetness impregnation. The synthesis mixture to prepare the embryonic zeolite comprised 9TPAOH:25SiO<sub>2</sub>:430 H<sub>2</sub>O:100EtOH. Tetrapropylammonium hydroxide (TPAOH) was used as template for all the synthesis [49]. The template was first mixed with distilled deionized water followed by addition of tetraethylorthosilicate (TEOS, Sigma-Aldrich, 98%) and homogenization of the mixture under stirring for 6 h resulting in water clear homogeneous sol solution. The resulted sol was subjected to a freeze-drying (-94 °C, under vacuum) to recover the embryonic zeolites. The obtained materials were redissolved in 0.5 M NH<sub>3</sub>NO<sub>3</sub> solution, stirred for 2 hours at room temperature followed by washing and drying in air.

### 2.2. Metal loading and sulfidation

The embryonic zeolite carriers were incipiently wetness impregnated with Mo-Co oxide precursors to prepare the materials. The total amount of Mo and Co in all catalysts was set at 5.0 wt.% for Mo, and from 1.0 to 1.7 wt.% for Co. In accordance with the content in metal, the materials were named: EZ<sub>Si</sub>-5%Mo, EZ<sub>Si</sub>-5%Mo-1%Co, and EZ<sub>Si</sub>-5%Mo-1.7%Co.

(NH<sub>4</sub>)<sub>6</sub>Mo<sub>7</sub>O<sub>24</sub>·4H<sub>2</sub>O was purchased from Alfa Aesar (99%) and used a precursor for molybdenum. Co(NO<sub>3</sub>)<sub>2</sub>·6H<sub>2</sub>O (Acros, 99%) was used a precursor for cobalt. The samples were first dried at room temperature followed by calcination at 550 °C for 5 h in static air. All the chemicals were used as received without any further purification.

30 ml/min, 10 vol% H<sub>2</sub>S in H<sub>2</sub> gas flow was used for the sulfidation of the samples. The treatment was performed in a Pyrex reactor on 300 mg of the fraction 35-45 mesh. The samples were first treated in N<sub>2</sub> flow at 140 °C for 2 h followed by heating up to 350 °C (2,8 °C·min<sup>-1</sup> ramp rate, in N<sub>2</sub> flow) and sulfidation treatment for 2 h. After the sulfidation, the samples were cooled down in N<sub>2</sub>. The flow of N<sub>2</sub> was maintained for 3 at room temperature before unloading of the samples.

### 2.3. Physicochemical characterization

The powder X-ray diffraction (PXRD) patterns were recorded on a PANalytical X'Pert Pro diffractometer using the Cu K $\alpha$  radiation ( $\lambda = 1.5418 \text{ \AA}$ ). The scanning electron micrographs were collected on a MIRA-LMH (Tescan) SEM equipped with a field emission gun.

The formation of the metal oxide and sulfide phases was monitored by Raman spectroscopy. The Raman spectra were acquired with a green laser at 532 nm (Jobin Yvon Labram 300 confocal Raman spectrometer coupled to a microscope and CCD detector). Both accumulation time and laser power were adjusted for the samples (embryonic zeolites after metal loading: 40-60 s accumulation 3 times at 50% laser power; after sulfidation: 15-25 s accumulation 3 times at 1% laser power).

Thermogravimetric analysis (TGA) was carried out with a SETSYS SETARAM analyzer. The temperature was increased from 30 to 800 °C at 5 °C/min in reconstituted (80 % N<sub>2</sub> + 20 % O<sub>2</sub>) dry air (40 mL/min).

XPS measurements of the samples were carried out in a SPECS spectrometer equipped with a PHOIBOS 150 MCD analyzer working at fixed pass energy of 35 eV and 0.1 eV resolution for the studied zones. Al K $\alpha$  radiation (1486.6 eV) was used at 250 W and 12.5 kV. Prior to analysis, each sample was pressed into a thin disk. All XPS spectra were recorded at room temperature. The analytical chamber operates under an ultra-high vacuum (10<sup>-10</sup> mbar). Binding energy correction was performed by fixing Si 2p at 103.4 eV corresponding to the unchanging zeolite support, and spectra were analyzed with CasaXPS software. To analyze the different Mo-species (MoO<sub>2</sub>, MoO<sub>3</sub>, Mo<sub>2</sub>C, MoS<sub>2</sub>) and the presence of coke or sulfur, high-definition spectra of the regions corresponding to S 2p, Mo 3d, O 1s, and C 1s levels were acquired and quantified.

### 2.4. Catalytic test

#### 2.4.1. General procedure

The catalytic performance test was conducted on a continuous fix-bed reactor in the temperature range of 700-750 °C, WHSV ranges 5.9-17.7 g(C<sub>2</sub>H<sub>6</sub>+CO<sub>2</sub>)/gcat × h<sup>-1</sup>, under atmospheric pressure. The feed was C<sub>2</sub>H<sub>6</sub>/CO<sub>2</sub> mixture with molar ratio between 1/0.74 with 10 v% of nitrogen as internal standard.

In a typical catalytic measurement, a total of 150-300 mg of the 100–400  $\mu\text{m}$  fraction of catalyst diluted was loaded into the middle of the reactor plugged by quartz wool on two sides. Before the catalytic test, the catalyst bed was pre-treated at 300 °C under an N<sub>2</sub> flow for 2 hours. The calibration of the flow rates was verified at 300 °C when no reaction occurred. Then the catalysts were heated up to the reaction temperature with a ramping rate of 10 °C/min in the flow of ethane and CO<sub>2</sub>. At the end of the test, the flow of the ethane and CO<sub>2</sub> was switched to nitrogen to cool down the reactor to the room temperature.

The effluents were analyzed online with a gas chromatograph (Interscience Compact GC) equipped with two TCDs and one FID. A Molsieve 5A, Rt-QBond, and Rtx-1 were used to separate light gases (H<sub>2</sub>, N<sub>2</sub>, CO, CO<sub>2</sub>), light hydrocarbons (CH<sub>4</sub>, C<sub>2</sub>H<sub>6</sub>, C<sub>2</sub>H<sub>4</sub>), and aromatics (from benzene till naphthalene), respectively. In all the experiments, N<sub>2</sub> was used as an internal standard to measure conversion and establish mass balance (Table S1).

Ethane conversion (C<sub>2</sub> conversion) and CO<sub>2</sub> (CO<sub>2</sub> conversion), ethylene selectivity (C<sub>2</sub>= selectivity), and CO selectivity (CO selectivity) were obtained as follows; the sum of the selectivities of the C<sub>3</sub>-C<sub>6</sub> fraction and aromatics was labeled heavies:

$$\text{Conversion}(i) = \frac{C_{\text{inlet}}(i) - C_{\text{outlet}}(i)}{C_{\text{inlet}}(i)} \cdot 100\%$$

$$\text{Carbon selectivity}(i) = \frac{F(i)}{\sum F(i)} \cdot 100\%$$

where  $F(i)$  is the mol of C in the product compound. The calculations as 'all C-contained products' were applied for tests, where CO was produced selectively (with significant contribution of DRE. CO is produced from CO<sub>2</sub> and C<sub>2</sub>H<sub>6</sub>); as 'C2-based products' (ethylene, methane, heavies) they were applied, where it was preferable ethylene production (ethane is converted to ethylene, methane, and heavies, CO<sub>2</sub> is converted to CO). Conversion and selectivities were calculated for the 200 min time-of -stream (TOS).

#### 2.4.2. Blank test (thermal test)

To avoid any performance artifact, the tests with the exact the same reaction mixtures but without any catalyst were performed (blank tests) in the range of the used by the study reaction conditions. The same starting procedure to the one, used in the experiments with the catalyst, was used. The blank test is also denoted as "thermal" test in the text.

### 3. Results and discussion

#### 3.1. Characterization of the catalysts

The embryonic zeolites are known as X-Ray amorphous materials with microporosity. It was previously demonstrated that after the metal loading, EZ's properties are conserved [5]. Metal-charged EZ was subjected to an XRD study. A low intense XRD peak around 26 °2 $\theta$  was observed for the bimetallic EZ<sub>Si</sub>-5%Mo-1%Co sample, which could be attributed to some polyoxide species (Fig. S1). The EDX mapping (Fig. S2) confirms that both metals are uniformly distributed on the embryonic support.

The formation of the oxidic phases was confirmed by Raman (Fig. S3). The Raman spectrum of EZ<sub>Si</sub>-5%Mo-1%Co shows different bands distribution with respect to monometallic EZ<sub>Si</sub>-5%Mo. While for the monometallic sample, the formation of  $\alpha$ -MoO<sub>3</sub> (990 and 821 cm<sup>-1</sup>) [50] phase is clearly visible, in the bimetallic sample, the bands of Mo–O–Mo and Mo–O<sub>t</sub> functionalities of [Mo<sub>7</sub>O<sub>24</sub>]<sup>6-</sup> polymolybdate species at 811, 870, and 937 cm<sup>-1</sup> are more intense [51,52]. The bands at 485 and 692 cm<sup>-1</sup> could be attributed to Co<sup>(II, III)</sup>O<sub>x</sub> [53].

The formation of the sulfidic precursor phase from oxidic is also monitored by Raman spectroscopy (Fig. S4). The bands at 370 and 404 cm<sup>-1</sup> are attributed to 2H-MoS<sub>2</sub>. The shoulder at 410 cm<sup>-1</sup> and the band at 441 cm<sup>-1</sup> are attributed to Co polysulfides.<sup>54</sup>

#### 3.2. Catalytic performances

##### 3.2.1. Role of cobalt promotion

A co-feeding experiment without a catalyst (Fig. 1) showed an ethane-to-ethylene conversion of about 14.2% with above 95% selectivity to ethylene. The CO<sub>2</sub> conversion was less than 2%. Our previous work showed that a Mo<sub>2</sub>C-supported catalyst could boost the CO<sub>2</sub> hydrogenation activity to CO. In other words, the Mo<sub>2</sub>C-supported catalyst catalyzes the reverse water-gas shift reaction (RWGS) without impacting the gas phase transformation of ethane to ethylene.<sup>5</sup> This ethane and CO<sub>2</sub> interaction pathway could be regarded as the ethylene production route (ethane dehydrogenation) accompanied by CO<sub>2</sub> hydrogenation (RWGS).<sup>55</sup> In total, these reactions were equivalent to ODH-CO<sub>2</sub>. However, the hydrogenation activity of the Mo<sub>2</sub>C catalyst remained limited due to reoxidation. In order to understand the impact of cobalt addition, Co-promoted bimetallic (EZ<sub>Si</sub>-(5%Mo<sub>2</sub>C-1%Co<sub>x</sub>C)<sub>s</sub>), Mo-based (EZ<sub>Si</sub>-(5%Mo<sub>2</sub>C)<sub>s</sub>), and Co-based (EZ<sub>Si</sub>-(5%Co<sub>x</sub>C)<sub>s</sub>) catalyst precursors were tested at 700 °C, with molar ratio ethane/CO<sub>2</sub>=1/0.74 at WHSV-5.9 h<sup>-1</sup> (Fig. 1).

On the Co-containing sample (EZ<sub>Si</sub>-(5%Co<sub>x</sub>C)<sub>s</sub>), a very different catalytic behavior was observed if compared with the Mo<sub>2</sub>C-supported catalyst. The conversions of CO<sub>2</sub> and ethane were significantly higher, about 26.4% and 19%, respectively, while the monometallic Mo-containing catalyst showed CO<sub>2</sub> conversion=9.7%, and ethane conversion=14.7%. However, in contrast to the Mo-containing sample, the Co-based system produced a significant amount of methane and reduced the yield of ethylene.

Interestingly, the results obtained on bimetallic EZ<sub>Si</sub>-(5%Mo<sub>2</sub>C-1%Co<sub>x</sub>C)<sub>s</sub> catalyst were very different from monometallic systems. CO<sub>2</sub> conversion was even further increased to the level of 70% as well as the conversion of ethane to about 32%. A clear synergetic effect between the two metals was observed. The selectivity pattern showed that a significant contribution of the DRE pathway occurs, which explains more than 3 times increased ethane conversion. Thus,

the ethane and CO<sub>2</sub> interaction pathway is an alternative to the ethylene route, where the C-C bond scissions were promoted instead of C-H bond scissions.

As DRE contribution was significant thus, a part of the ethane carbons is transformed to CO, complementing those obtained from CO<sub>2</sub>. The ethylene yield and CO/ethylene molar ratio obtained on the different catalysts were compared (Fig. 1). One can see that ethylene yield is very close to the ethane conversion in the thermal conversion without catalyst and over Mo<sub>2</sub>C-supported catalyst. In contrast, the Co-contained samples tended to produce CO under the same reaction conditions. The molar ratio of CO/C<sub>2</sub>H<sub>6</sub> significantly higher than 1 confirmed the prevalence of DRE to RWGS for the CO<sub>2</sub> conversion route. The Mo-Co-based sample was more prone to CO production than others. During the non-catalytic 'thermal' test, CO was almost absent in the product slate.

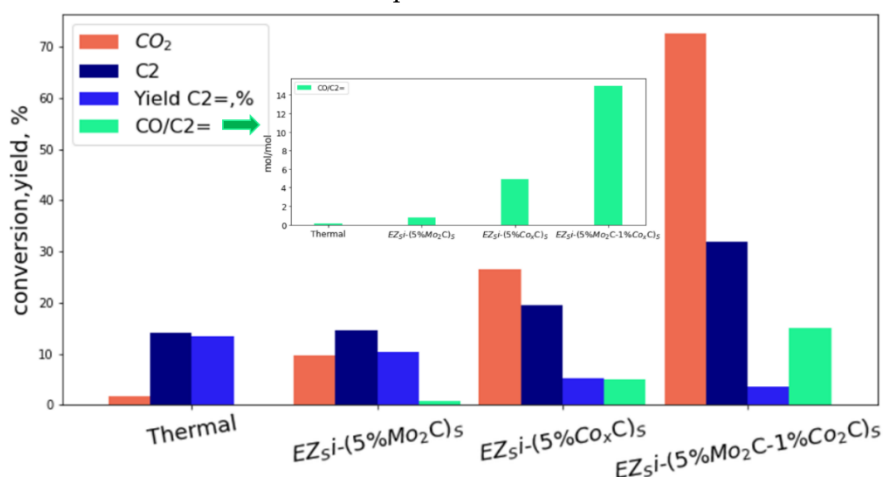


**Fig. 1.** Ethane (C<sub>2</sub>) co-processing with CO<sub>2</sub> on catalysts (C<sub>2</sub>): average conversion of CO<sub>2</sub> and ethane, ethylene yield, and molar ratio produced CO/C<sub>2</sub>= as the process descriptor (coke-free basis, T=700 °C, P=1 atm, C<sub>2</sub>H<sub>6</sub>/CO<sub>2</sub>=1/0.74, WHSV=5.9 h<sup>-1</sup>). Insert - Enlarged and detached CO/C<sub>2</sub> = molar ratio.

### 3.2.2. Impact of operating conditions

The first tests in co-processing CO<sub>2</sub> with ethane showed the synergetic effect of cobalt and molybdenum. The significantly higher catalyst activity was recorded but at the expense of selectivity. In order to optimize the process, the effect of the weight hourly space velocity (WHSV) and the reaction temperature was studied.

In the case of the reaction proceeding along the route for ethylene production, CO is obtained substantially by CO<sub>2</sub> hydrogenation (RWGS) with a selectivity close to 100%<sup>5</sup> without any significant DRE contribution. Under the conditions favoring ethylene formation, the selectivities of the non-catalytic (thermal) and catalytic processes were compared on a C<sub>2</sub>-products basis. The selectivities calculations as 'all C-contained products' were applied for comparison with the experiments, where CO was registered as the preferred product.

The bimetallic catalyst (EZ<sub>Si</sub>-(5%Mo<sub>2</sub>C-1%Co<sub>x</sub>C)<sub>s</sub>) was tested at 700 °C at two WHSV values - 5.9 to 11.8 h<sup>-1</sup> (Fig. 2a, b). The data in Fig. 2 shows that the change of WHSV resulted in a dramatic selectivity change and suppression of the DRE pathway. Ethylene has become the main product at higher WHSV. The selectivity pattern becomes again very similar to the one of ODH-CO<sub>2</sub>. This could indicate that the ethylene undergoes further transformation on the catalytic surface and reacts with CO<sub>2</sub> resulting in additional CO formation.

A series of experiments were performed at 750 °C, with WHSV 11.8 and 17.7 h<sup>-1</sup> at the same molar ratio of C<sub>2</sub>H<sub>6</sub>/CO<sub>2</sub>=1/0.74 (Fig. 2c, d). In contrast to 700 °C, the most abandoned product at WHSV=11.8 h<sup>-1</sup> was CO. However, an increase of the WHSV to 17.7 h<sup>-1</sup> immediately changed the selectivity to the ethylene production route accompanied by RWGS. At WHSV=17.7 h<sup>-1</sup>, CO<sub>2</sub> conversion (33.6%) was lower than for ethane (41.3%). The effluent flow contained mostly ethylene, some methane, and heavies in addition to the CO released from the CO<sub>2</sub> hydrogenation (RWGS). This result suggests that ethylene is an intermediate compound that reacts with CO<sub>2</sub> at a higher conversion level (Fig. 2d). The conversion of CO<sub>2</sub> and ethane at WHSV=5.9 h<sup>-1</sup>, T=700 °C as a function of TOS is presented in Fig. S5. Some decrease of CO<sub>2</sub> conversion was observed while C<sub>2</sub> conversion remained stable in TOS.

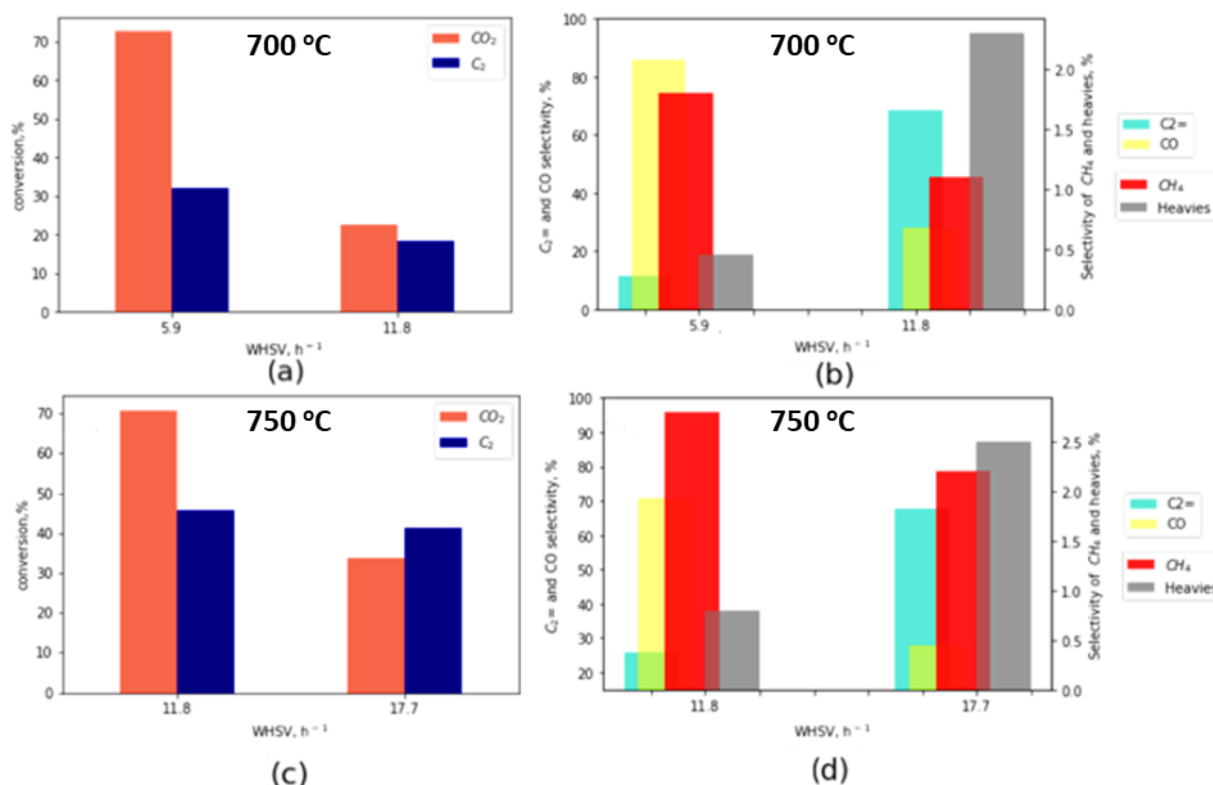


**Fig. 2.** Ethane (C<sub>2</sub>) co-processing with CO<sub>2</sub> on EZ<sub>Si</sub>-(5%Mo<sub>2</sub>C-1%Co)<sub>x</sub>S: a and c- average conversion of CO<sub>2</sub> and ethane; b and d- all C-products selectivities (coke-free basis) as a function of WHSV, h<sup>-1</sup> (a-b: T=700 °C and c-d: T=750 °C, P=1 atm, C<sub>2</sub>H<sub>6</sub>/CO<sub>2</sub>=1/0.74).

In brief, WHSV variations on bimetallic samples allow adjusting the product selectivity. At higher WHSV and lower contact time, the process is set to ethylene production (ODH-CO<sub>2</sub>). Thus, the product selectivity distribution proves that an increase in WHSV prevents transformation via dry reforming. In contrast, at lower WHSV, the process is more selective to CO production. Therefore, the pathway of DRE prevails.

In order to compare the catalyst performance of the monometallic and bimetallic catalysts, the data were linearly extrapolated to the same level of conversion of ethane (18.2%) (Fig. 3a). It was equivalent to a temperature increase of about 7 °C for a monometallic sample. The comparison was performed on ethane-based selectivity. The sum of the methane and heavy fractions selectivity was higher for EZ<sub>Si</sub>-(5%Mo<sub>2</sub>C-1%Co)<sub>x</sub>S and equaled about 3% in contrast to about 2% on Mo<sub>2</sub>C-supported catalyst. In contrast, the bimetallic catalyst showed higher conversion in CO<sub>2</sub> hydrogenation of about 20% vs. about 15% on EZ<sub>Si</sub>-(5%Mo<sub>2</sub>C)<sub>s</sub>. Importantly, the same conversion level of ethane with roughly similar selectivity could be reached on a Co-promoted catalyst at a 7 °C lower temperature and shorter contact time without substantial loss in selectivity.

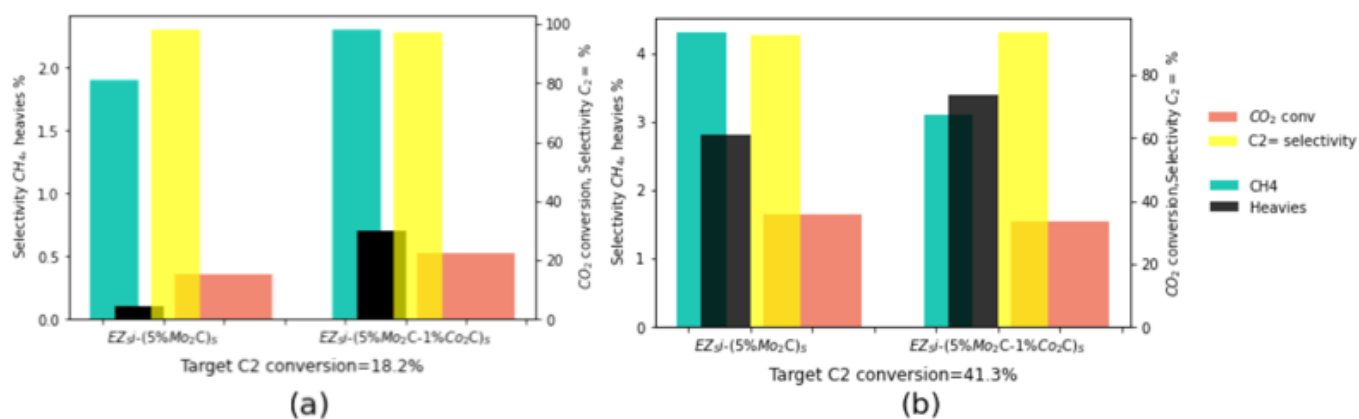


**Fig. 3.** (a) Comparison of catalysts EZ<sub>Si</sub>-5%(Mo<sub>2</sub>C)<sub>s</sub> and EZ<sub>Si</sub>-(5%Mo<sub>2</sub>C-1%Co)<sub>x</sub>S in ODH-CO<sub>2</sub> of ethane at the same conversion level of ethane 18.2%; (b) at the same conversion level of ethane 41.3%. (coke-free basis, a: T=700 °C, b:

T = 750 °C, P = 1 atm, C<sub>2</sub>H<sub>6</sub>/CO<sub>2</sub> = 1/0.74, C<sub>2</sub>-based selectivities). Note - for EZ<sub>Si</sub>-(5%Mo<sub>2</sub>C)<sub>s</sub>, the results were extrapolated at 710 °C (conversion 18.2%) and at 753 °C (conversion 41.3%).

Similarly, the performance of EZ<sub>Si</sub>-(5%Mo<sub>2</sub>C-1%Co<sub>x</sub>C)<sub>s</sub> catalyst at 750 °C and WHSV=17.7 h<sup>-1</sup> was compared with the extrapolated performances of the monometallic EZ<sub>Si</sub>-(5%Mo<sub>2</sub>C)<sub>s</sub> (WHSV=5.9 h<sup>-1</sup>) (Fig. 3b). The comparison was performed at the conversion level of ethane (41.3%). One can see that the selectivity pattern was very similar but at three times shorter contact time. We interpret this result as proof that the cobalt doesn't modify the active sites' nature. In other words, Co-addition stabilizes the Mo<sub>2</sub>C active phase and boosts the activity of the catalyst without a significant change in selectivity due to better utilization of the Mo-loaded counterparts.

### 3.3. Study of the spent catalysts

#### 3.3.1. XRD study

The effect of cobalt loading on the resistance of catalysts to oxidation and preventing MoO<sub>2</sub> formation was studied. According to the XRD results, the stability of the Mo<sub>2</sub>C species to reoxidation on Co-promoted materials significantly increased, compared with the monometallic system (Fig. 4). For the spent EZ<sub>Si</sub>-(5%Mo<sub>2</sub>C-1%Co<sub>x</sub>C)<sub>s</sub>-750 (WHSV=11.8 h<sup>-1</sup>), and EZ<sub>Si</sub>-(5%Mo<sub>2</sub>C-1%Co<sub>x</sub>C)<sub>s</sub>-750 (WHSV=17.7 h<sup>-1</sup>) catalysts, the XRD study did not reveal MoO<sub>2</sub> presence in the carbide phase. Typically, MoO<sub>2</sub> for this type of catalyst appeared by intense peaks at 26, triplets at 37.4, and 53.5°. This XRD signature was observed for the spent monometallic sample. For the bimetallic sample tested at lower WHSV (selective CO production), an intense peak at 26° was registered. However, a triplet around 37° two theta or other MoO<sub>2</sub> characteristic peaks was not detected. Therefore, this peak has a different nature. The SEM inspection revealed the presence of carbon nanotubes (CNTs) (Fig. 5). In general, well-graphitized multi-wall CNTs (MWCNT) show peaks at 26° (002) [56], 42-44° (100) [57, 58], 53° (004) and 78° (110).

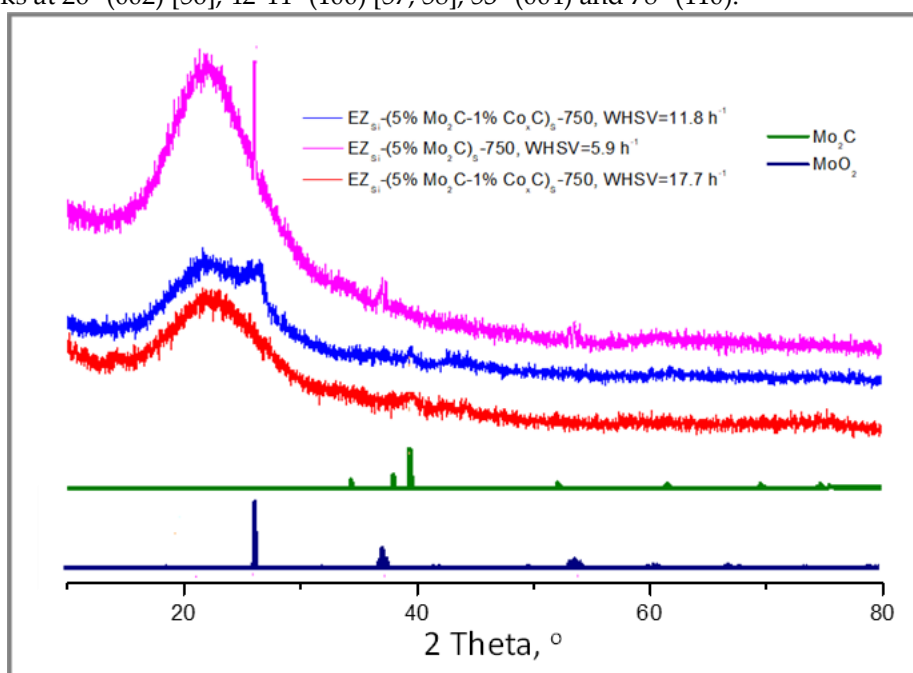


**Fig. 4.** XRD patterns of spent monometallic (EZ<sub>Si</sub>-(5%Mo<sub>2</sub>C)<sub>s</sub>) and bimetallic (EZ<sub>Si</sub>-(5%Mo<sub>2</sub>C-1%Co<sub>x</sub>C)<sub>s</sub>) catalysts at 750 °C. Mo<sub>2</sub>C simulated from the cif of crystal with orthorhombic Pbcn space group [59], MoO<sub>2</sub> pattern simulated from the cif of monoclinic crystal with P21/c space group [60].

XRD peaks of the Mo<sub>2</sub>C phase show low intensity. We attribute this feature to the EZ carriers, which limits the growth of Mo<sub>2</sub>C. Also, the carbide particle size is limited due to the nature of the carburization agent [61]. However, some bulkier particle formation is still possible. In other words, particles' aggregation might occur due to the formation of MoO<sub>2</sub> on the particles' surface. Still, our data show that the Co-promoting reduces the rate of carbide oxidation to oxide and thus stabilizes the catalyst composition. This is confirmed by the nature spent bimetallic samples pattern.

The formation of filamentous carbon containing some CNT species was observed only on Co-promoted samples (Fig. 5). The amount of CNT was highest under CO preferential formation conditions (Fig. 5b) and most probably

originates from the ethylene conversion [62,63]. The CNT-like species formation was almost not observed on the bimetallic catalyst under the conditions favoring ethylene production (Fig. 5c).

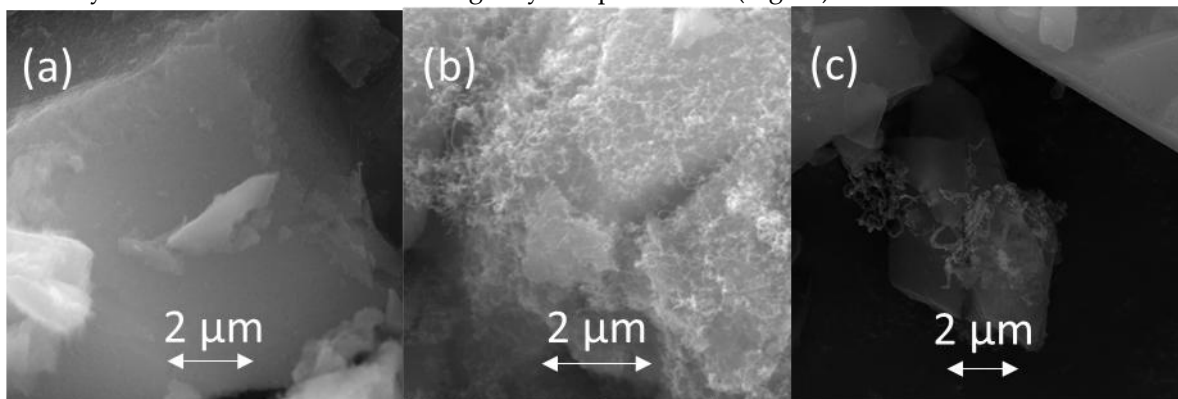


**Fig. 5.** SEM images of the spent samples: (a)  $EZ_{Si}-(5\%Mo_2C)_S-750$ ,  $WHSV=5.9\ h^{-1}$ , (b)  $EZ_{Si}-(5\%Mo_2C-1\%Co_xC)_S-750$ ,  $WHSV=11.8\ h^{-1}$ , and (c)  $EZ_{Si}-(5\%Mo_2C-1\%Co_xC)_S$ ,  $WHSV=17.7\ h^{-1}$ .

**3.3.2. TG study.** The TGA curves measured for monometallic and bimetallic spent catalysts are given in Fig. 6. All  $Mo_2C$ -containing samples demonstrated a slight weight increase up to  $470\ ^\circ C$  due to the oxidation reaction of  $Mo_2C$  to  $MoO_3$ . The weight loss above  $470\ ^\circ C$  corresponded to deposit carbon combustion.

One of the bimetallic samples ( $EZ_{Si}-(5\%Mo_2C-1\%Co_xC)_S$ ) was tested under conditions favoring ethylene production ( $WHSV=17.7\ h^{-1}$ ). The same bimetallic sample was tested under conditions favoring CO production ( $WHSV=11.8\ h^{-1}$ ). These results were compared with the TG curve of the spent monometallic  $EZ_{Si}-(5\%Mo_2C)_S$  ( $WHSV=5.9\ h^{-1}$ ) catalyst at  $750\ ^\circ C$  (Fig. 6). The total weight loss for the bimetallic sample tested at  $WHSV=11.8\ h^{-1}$  was much higher than for the two other samples. Therefore, the bimetallic sample favors the coke formation when it generates ethylene in a lower concentration. Moreover, the deposited carbon was in the form of CNTs (Fig. 5b). However, it was not possible to quantify the percentage of coke and nanotubes.

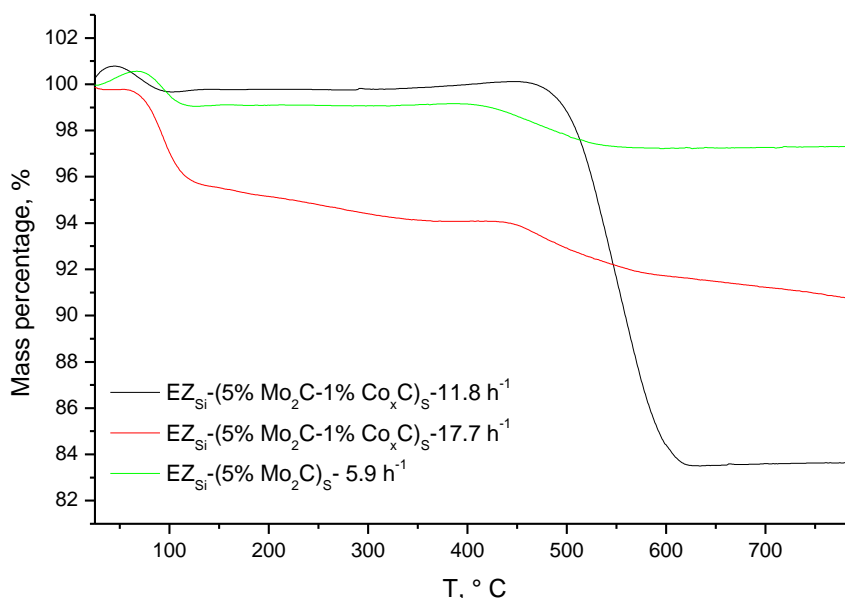


**Fig. 6.** Thermogravimetric analysis of spent  $EZ_{Si}-(5\%Mo_2C-1\%Co_xC)_S$  and  $EZ_{Si}-(5\%Mo_2C)_S$  spent at  $750\ ^\circ C$ .

### 3.3.3. XPS study

XPS measurements were performed for samples spent at  $750\ ^\circ C$  to verify a carbide phase presence. Monometallic and bimetallic samples were compared under various conditions: favoring CO or ethylene formation. The observed peaks are characteristic of Mo (3d), C (1s), O (1s), Si (2s), and S (2s).

The XPS spectra of the samples are presented in Fig. S6, while the high-resolution spectra of Mo (3d) and C (1s) are depicted in Fig. 7. The presence of the carbide and oxide phase was identified by the Mo (3d) high-resolution spectrum, where a complex peak was obtained. To estimate the contribution of different components, a deconvolution using

CASA software was carried out, considering that all the species should provide a doublet in proportion 2:3 corresponding to  $3d_{3/2}$  and  $3d_{5/2}$ , and the energy gap between them should be in 3.1 – 3.2 eV range. The peaks centered at 231.5 and 235 eV could be assigned to  $3d_{5/2}$  and  $3d_{3/2}$  of  $Mo^{6+}$ , respectively, while those around 228 and 231.3 eV to  $3d_{5/2}$  and  $3d_{3/2}$  of  $Mo^{4+}$ , and the ones at 223.8 and 227 to  $3d_{5/2}$  and  $3d_{3/2}$  of  $Mo^{2+}$ . The  $Mo^{4+}$  presence could be matched with the  $MoO_2$  phase, while  $Mo^{6+}$  emanates from  $MoO_3$  obtained from metastable  $MoO_2$  during the analysis. The analysis of the Si (2s)+S (2p) (Fig. S7) and Mo (3d)+S (2s) ranges do not indicate the presence of sulfur, while  $Mo^{4+}$  could not be attributed to  $MoS_2$ . Therefore, the  $Mo^{2+}$  presence could be accepted as evidence of  $Mo_2C$  presence. The O 1s spectrum (Fig. S8) also displays one peak at 531.5 eV corresponding to Si-O-Si and Mo-O.

The observation of the three oxidation states of Mo suggests the presence of  $MoO_3$  ( $Mo^{6+}$ ),  $MoO_4$  and/or  $MoS_2$  ( $Mo^{4+}$ ), and  $Mo_2C$  ( $Mo^{2+}$ ). The O, C, and S species were also analyzed to verify these assumptions. In the case of O (1s) (Fig. S8), the presence of oxide-based compounds is indistinguishable; the peak centered at 531.5 eV could correspond to both Si-O-Si and Mo-O<sub>x</sub> oxides. On the contrary, in the analysis of C (1s) (Fig. 7), the presence of a shoulder or second peak at lower binding energy (c.a. 279.4 eV) with respect to the usual peak at 284.6 eV indicates the formation of carbides, supporting the formation of  $Mo_2C$ . Finally, to distinguish between  $MoO_4$  and  $MoS_2$ , S (2p) was analyzed. The absence of S (2p) (at c.a. 162.1 eV, Fig. S7) allows for attributing the  $Mo^{4+}$  to the formation of  $MoO_4$ .

From the C (1s) spectra analysis, two peaks around 280 and 283.2 eV are identified (Fig. 7). A peak around 280 eV corresponds to C bonded to Mo, and the one around 283.2 eV is associated with C-C. Based on the ratio between these peaks (Fig. 7), the following trend can be traced - for cobalt-promoted samples, the carbon content in the carbide phase is equal to or higher than in the coke. Thus, this further confirms the assumption that the proportion of coke in carbon deposits is significantly reduced for bimetallic samples.

The addition of cobalt to the Mo-containing catalysts contributes to preserving the carbide phase oxidation to molybdenum oxide species under the reaction conditions and reduces carbon deposition on the catalyst. Molybdenum oxide species are inactive neither in  $CO_2$  hydrogenation nor in ethane dehydrogenation. So, the Co-promoted samples allow maintaining higher concentration of the carbide species during the reaction vs. monometallic catalysts, resulting in much higher catalyst activity and in achieving the same conversion level at milder conditions (lower temperature, shorter contact times). However, the selectivity at the same conversion level remains the same for both Co-promoted and monometallic catalysts, what could be due to the similar nature of the active sites on both catalysts.

#### 4. Conclusions

Mo-Co carbide supported on all-silica embryonic zeolites showed significantly higher activity in ODH- $CO_2$  in contrast to the monometallic sample without any substantial impact on selectivity to ethylene. In addition, co-promoting led to improving both dehydrogenative and hydrogenative properties.

By adjustment of the operating conditions, the cobalt-promoted  $Mo_2C$  system can favor either DRE or ODH- $CO_2$  reaction pathways, in other words, for CO and ethylene production, on the same catalyst.

Co-promoting has several positive effects on  $Mo_2C$ -based catalysts' stability. First, it prevents fast catalyst surface oxidation by the  $CO_2$  to  $MoO_2$  phase, which is not active in hydrogenation. The formation of  $MoO_2$  is mainly responsible for particle agglomeration, which eventually results in irreversible deactivation. Second, promoting with cobalt decreases carbon accumulation on the catalyst surface. Thus, Co-promoting of the Mo-carbide system resolves the issue of lower activity and allows mitigating catalyst deactivation in  $CO_2$  coprocessing with ethane.

Carbon circularity through co-processing  $CO_2$  with ethane over Co-promoted supported Mo-carbide systems opens new perspectives in  $CO_2$ -neutral chemical production.

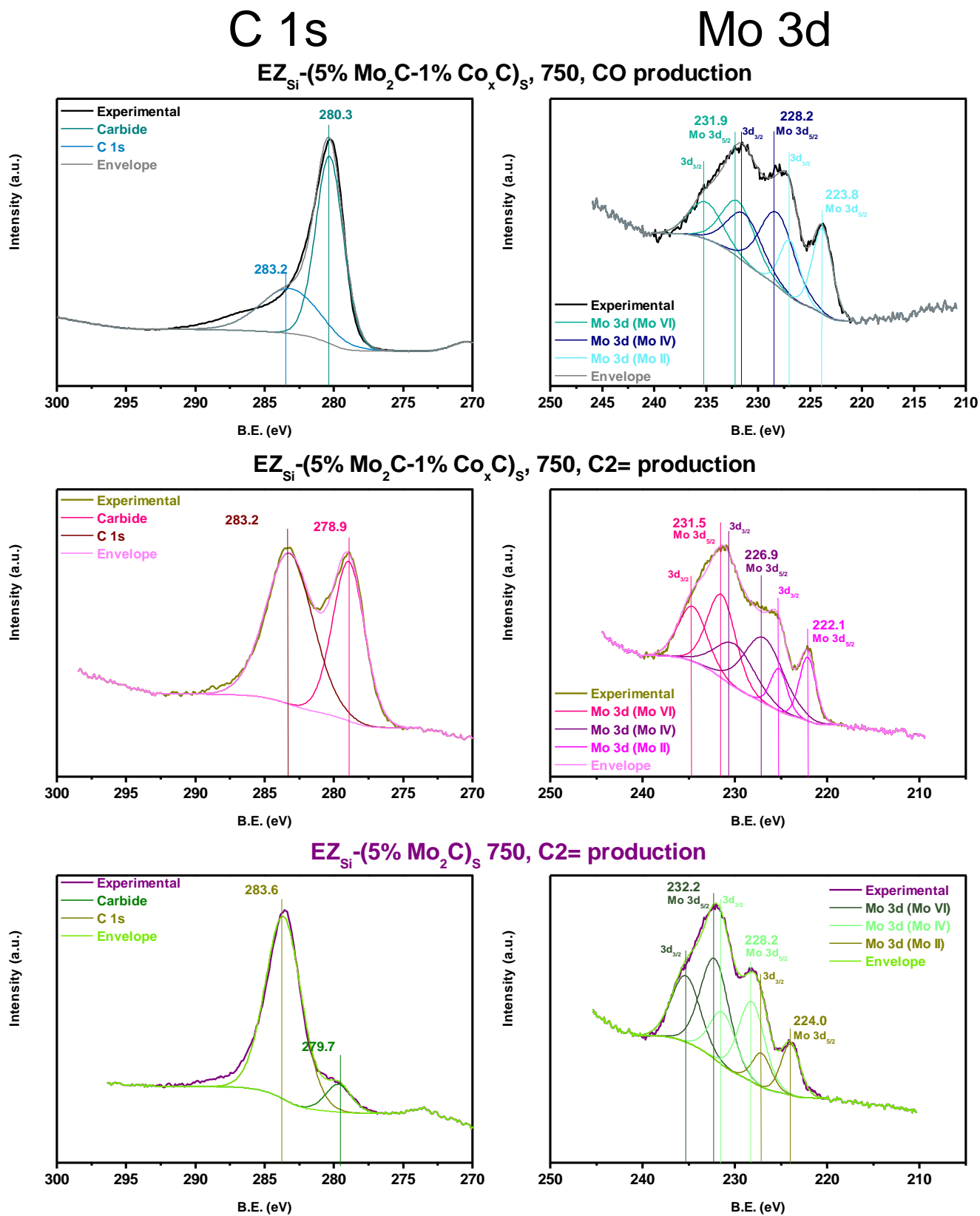


**Fig. 7.** XPS high-resolution spectra of C 1s (left) Mo 3d (right) of EZ<sub>Si</sub>-(5%Mo<sub>2</sub>C-1%Co<sub>x</sub>C)<sub>s</sub>: applied for CO selective production (EZ<sub>Si</sub>-(5%Mo<sub>2</sub>C-1%Co<sub>x</sub>C)<sub>s</sub>, 750, WHSV=11.8h<sup>-1</sup>), and ethylene production (EZ<sub>Si</sub>-(5%Mo<sub>2</sub>C-1%Co<sub>x</sub>C)<sub>s</sub>, 750, WHSV=17.7h<sup>-1</sup>), and EZ<sub>Si</sub>-(5%Mo<sub>2</sub>C)<sub>s</sub> (WHSV=5.9 h<sup>-1</sup>).

**Declaration of competing interest**

The authors declare that they have no known competing financial interests or personal relationships that could have appeared to influence the work reported in this paper.

## Acknowledgments

This research was supported by TotalEnergies, the Industrial Chair ANR-TOTAL “NanoClean Energy” [ANR-17-CHIN-0005-01] and project NanoCleanEnergy+ (Region Normandy). The authors thank the general research services center CITIUS for the XPS measurements.

## Author Contributions

Vera Bikbaeva: Investigation, Methodology, Writing - Original Draft. Nikolay Nesterenko: Conceptualization, Supervision, Reviewing and Editing. Nuria García-Moncada: Investigation, Valentin Valtchev: Conceptualization, Supervision, Reviewing and Editing.

## Supplementary Material

Summary of the supplementary information:

Fig. S1: XRD patterns of EZ<sub>Si</sub>-5%Mo (WI), EZ<sub>Si</sub>-9%Mo (HT), EZ<sub>Si</sub>-5%MoO<sub>3</sub>-1%CoO<sub>x</sub> and EZ<sub>Si</sub>-5%MoO<sub>3</sub>-1.7%CoO<sub>x</sub>;

Fig. S2: EDX elemental mapping of Mo and Co in EZ<sub>Si</sub>-5%Mo-1%Co: Mo (a) and Co (b).

Fig. S3: Raman spectrum of EZ decorated with a) Mo oxide prepared by wetness impregnation (WI) and hydrothermal treatment (HT); b) Mo and Co oxide prepared by wetness impregnation (WI) and compared with EZ decorated with a Mo oxide (WI).

Fig. S4: Raman spectrum of EZ decorated with a) Mo oxide prepared by wetness impregnation (WI) and hydrothermal treatment (HT); b) Mo and Co oxide prepared by wetness impregnation (WI) and compared with EZ decorated with a Mo oxide (WI).

Fig. S5: CO<sub>2</sub> and C<sub>2</sub> conversion as the function of time on stream (TOS) on EZ<sub>Si</sub>-(5%Mo<sub>2</sub>C-1%Co<sub>x</sub>C)<sub>s</sub> (700 °C, WHSV=5.9 h<sup>-1</sup>, P=1 atm, and C<sub>2</sub>H<sub>6</sub>/CO<sub>2</sub>=1/0.74).

Fig. S6: XPS analysis spectra of EZ<sub>Si</sub>-(5%Mo<sub>2</sub>C-1%Co<sub>x</sub>C)<sub>s</sub> applied for selective CO production (EZ<sub>Si</sub>-(5%Mo<sub>2</sub>C-1%Co<sub>x</sub>C)<sub>s</sub>, WHSV=11.8 h<sup>-1</sup>), applied for selective ethylene production (EZ<sub>Si</sub>-(5%Mo<sub>2</sub>C-1%Co<sub>x</sub>C)<sub>s</sub>, WHSV=17.7 h<sup>-1</sup>), and EZ<sub>Si</sub>-(5%Mo<sub>2</sub>C)<sub>s</sub> (WHSV=5.9 h<sup>-1</sup>). All samples were characterized after catalytic tests at 750 °C.

Fig. S7: XPS high resolution spectra Si 2s of EZ<sub>Si</sub>-(5%Mo<sub>2</sub>C-1%Co<sub>x</sub>C)<sub>s</sub> applied for selective CO production (EZ<sub>Si</sub>-(5%Mo<sub>2</sub>C-1%Co<sub>x</sub>C)<sub>s</sub>, WHSV=11.8 h<sup>-1</sup>), applied for selective ethylene production (EZ<sub>Si</sub>-(5%Mo<sub>2</sub>C-1%Co<sub>x</sub>C)<sub>s</sub>, WHSV=17.7 h<sup>-1</sup>), and EZ<sub>Si</sub>-(5%Mo<sub>2</sub>C)<sub>s</sub> (WHSV=5.9 h<sup>-1</sup>). All samples were characterized after catalytic tests at 750 °C.

Fig. S8: XPS high resolution spectra O 1s of EZ<sub>Si</sub>-(5%Mo<sub>2</sub>C-1%Co<sub>x</sub>C)<sub>s</sub> applied for selective CO production (EZ<sub>Si</sub>-(5%Mo<sub>2</sub>C-1%Co<sub>x</sub>C)<sub>s</sub>, WHSV=11.8 h<sup>-1</sup>), applied for selective ethylene production (EZ<sub>Si</sub>-(5%Mo<sub>2</sub>C-1%Co<sub>x</sub>C)<sub>s</sub>, WHSV=17.7 h<sup>-1</sup>), and EZ<sub>Si</sub>-(5%Mo<sub>2</sub>C)<sub>s</sub> (WHSV=5.9 h<sup>-1</sup>). All samples were characterized after catalytic tests at 750 °C.

## References

[1] Climate Change 2022: Mitigation of Climate Change. <https://www.ipcc.ch/report/ar6/wg3/> (accessed January 23, 2023).

[2] The Future of Petrochemicals 2021, International Energy Agency report. <https://www.iea.org/reports/the-future-of-petrochemicals>.

[3] Global Energy Review 2021 – Analysis, IEA. <https://www.iea.org/reports/global-energy-review-2021> (accessed January 24, 2023).

- [4] Artificial photosynthesis for greener ethylene production. <https://www.electronicsspecifier.com/products/renewables/artificial-photosynthesis-for-greener-ethylene-production> (accessed January 29, 2023).
- [5] V. Bikbaeva, N. Nesterenko, S. Konnov, T.-S. Nguyen, J.-P. Gilson, V. Valtchev, A low carbon route to ethylene: Ethane oxidative dehydrogenation with CO<sub>2</sub> on embryonic zeolite supported Mo-carbide catalyst, *Applied Catalysis B: Environmental*. 320 (2023) 122011. <https://doi.org/10.1016/j.apcatb.2022.122011>.
- [6] V. Bikbaeva, O. Perez, N. Nesterenko, V. Valtchev, Ethane oxidative dehydrogenation with CO<sub>2</sub> on thiogallates, *Inorg. Chem. Front.* (2022) 10.1039/D2QI01630C. <https://doi.org/10.1039/D2QI01630C>.
- [7] E.R. <https://www.emergenresearch.com>, Syngas Market Trend | Synthesis Gas Industry Forecast 2021-2030. <https://www.emergenresearch.com/amp/industry-report/syngas-market> (accessed January 23, 2023).
- [8] Y. Wang, K. Wang, B. Zhang, X. Peng, X. Gao, G. Yang, H. Hu, M. Wu, N. Tsubaki, Direct Conversion of CO<sub>2</sub> to Ethanol Boosted by Intimacy-Sensitive Multifunctional Catalysts, *ACS Catal.* 11 (2021) 11742–11753. <https://doi.org/10.1021/acscatal.1c01504>.
- [9] O.A. Ojelade, S.F. Zaman, A review on CO<sub>2</sub> hydrogenation to lower olefins: Understanding the structure-property relationships in heterogeneous catalytic systems, *Journal of CO<sub>2</sub> Utilization*. 47 (2021) 101506. <https://doi.org/10.1016/j.jcou.2021.101506>.
- [10] N. Nesterenko, J. Aguilhon, Ph. Bodart, D. Minoux, J.-P. Dath, Methanol to Olefins, in: *Zeolites and Zeolite-Like Materials*, Elsevier, 2016: pp. 189–263. <https://doi.org/10.1016/B978-0-444-63506-8.00006-9>.
- [11] W. Cho, H. Yu, Y. Mo, CO<sub>2</sub> Conversion to Chemicals and Fuel for Carbon Utilization, in: Y. Yun (Ed.), *Recent Advances in Carbon Capture and Storage*, InTech, 2017. <https://doi.org/10.5772/67316>.
- [12] S.C. Arnold, A.M. Gaffney, R. Song, C.Y. Yeh, Process for producing ethylene via oxidative dehydrogenation (ODH) of ethane, US8519210B2, 2013.
- [13] F. Cavani, N. Ballarini, A. Cericola, Oxidative dehydrogenation of ethane and propane: How far from commercial implementation?, *Catalysis Today*. 127 (2007) 113–131. <https://doi.org/10.1016/j.cattod.2007.05.009>.
- [14] T. Yabe, Y. Sekine, Methane conversion using carbon dioxide as an oxidizing agent: A review, *Fuel Processing Technology*. 181 (2018) 187–198. <https://doi.org/10.1016/j.fuproc.2018.09.014>.
- [15] M. González-Castaño, B. Dorneanu, H. Arellano-García, The reverse water gas shift reaction: a process systems engineering perspective, *React. Chem. Eng.* (2021) 954–976. <https://doi.org/doi.org/10.1039/D0RE00478B>.
- [16] C.-S. Chen, W.-H. Cheng, S.-S. Lin, Study of reverse water gas shift reaction by TPD, TPR and CO<sub>2</sub> hydrogenation over potassium-promoted Cu/SiO<sub>2</sub> catalyst, *Applied Catalysis A: General*. 238 (2003) 55–67. [https://doi.org/10.1016/S0926-860X\(02\)00221-1](https://doi.org/10.1016/S0926-860X(02)00221-1).
- [17] S.S. Kim, H.H. Lee, S.C. Hong, A study on the effect of support's reducibility on the reverse water-gas shift reaction over Pt catalysts, *Applied Catalysis A: General*. 423–424 (2012) 100–107. <https://doi.org/10.1016/j.apcata.2012.02.021>.
- [18] S.S. Kim, K.H. Park, S.C. Hong, A study of the selectivity of the reverse water-gas-shift reaction over Pt/TiO<sub>2</sub> catalysts, *Fuel Processing Technology*. 108 (2013) 47–54. <https://doi.org/10.1016/j.fuproc.2012.04.003>.
- [19] J.H. Kwak, L. Kovarik, J. Szanyi, CO<sub>2</sub> Reduction on Supported Ru/Al<sub>2</sub>O<sub>3</sub> Catalysts: Cluster Size Dependence of Product Selectivity, *ACS Catal.* 3 (2013) 2449–2455. <https://doi.org/10.1021/cs400381f>.
- [20] A. Ranjbar, A. Irankhah, S.F. Aghamiri, Reverse water gas shift reaction and CO<sub>2</sub> mitigation: nanocrystalline MgO as a support for nickel based catalysts, *Journal of Environmental Chemical Engineering*. 6 (2018) 4945–4952. <https://doi.org/10.1016/j.jece.2018.07.032>.
- [21] L. Deng, X. Ai, F. Xie, G. Zhou, Efficient Ni-based catalysts for low-temperature reverse water-gas shift (RWGS) reaction, *Chem. Asian J.* 16 (2021) 949–958. <https://doi.org/10.1002/asia.202100100>.

- [22] A.G. Kharaji, A. Shariati, M. Ostadi, Development of Ni–Mo/Al<sub>2</sub>O<sub>3</sub> Catalyst for Reverse Water Gas Shift (RWGS) Reaction, *J Nanosci Nanotechnol.* 14 (2014) 6841–6847. <https://doi.org/10.1166/jnn.2014.8962>.
- [23] H. Jing, Q. Li, J. Wang, D. Liu, K. Wu, Theoretical Study of the Reverse Water Gas Shift Reaction on Copper Modified  $\beta$ -Mo<sub>2</sub>C(001) Surfaces, *J. Phys. Chem. C.* 123 (2019) 1235–1251. <https://doi.org/10.1021/acs.jpcc.8b09884>.
- [24] Q. Zhang, L. Pastor-Pérez, W. Jin, S. Gu, T.R. Reina, Understanding the promoter effect of Cu and Cs over highly effective  $\beta$ -Mo<sub>2</sub>C catalysts for the reverse water-gas shift reaction, *Applied Catalysis B: Environmental.* 244 (2019) 889–898. <https://doi.org/10.1016/j.apcatb.2018.12.023>.
- [25] Y. Ma, Z. Guo, Q. Jiang, K.-H. Wu, H. Gong, Y. Liu, Molybdenum carbide clusters for thermal conversion of CO<sub>2</sub> to CO via reverse water-gas shift reaction, *Journal of Energy Chemistry.* 50 (2020) 37–43. <https://doi.org/10.1016/j.jechem.2020.03.012>.
- [26] A. Pajares, X. Liu, J.R. Busacker, P. Ramírez de la Piscina, N. Homs, Supported Nanostructured Mo<sub>x</sub>C Materials for the Catalytic Reduction of CO<sub>2</sub> through the Reverse Water Gas Shift Reaction, *Nanomaterials.* 12 (2022) 3165. <https://doi.org/10.3390/nano12183165>.
- [27] K.P. Reddy, S. Dama, N.B. Mhamane, M.K. Ghosalya, T. Raja, C.V. Satyanarayana, C.S. Gopinath, Molybdenum carbide catalyst for the reduction of CO<sub>2</sub> to CO: surface science aspects by NAPPEs and catalysis studies, *Dalton Trans.* 48 (2019) 12199–12209. <https://doi.org/10.1039/C9DT01774G>.
- [28] W. Marquart, S. Raseale, G. Prieto, A. Zimina, B.B. Sarma, J.-D. Grunwaldt, M. Claeys, N. Fischer, CO<sub>2</sub> Reduction over Mo<sub>2</sub>C-Based Catalysts, *ACS Catal.* 11 (2021) 1624–1639. <https://doi.org/10.1021/acscatal.0c05019>.
- [29] W. Marquart, M. Claeys, N. Fischer, Conversion of CO<sub>2</sub> and small alkanes to platform chemicals over Mo<sub>2</sub>C-based catalysts, *Faraday Discuss.* 230 (2021) 68–86. <https://doi.org/10.1039/D0FD00138D>.
- [30] S. Yao, B. Yan, Z. Jiang, Z. Liu, Q. Wu, J.H. Lee, J.G. Chen, Combining CO<sub>2</sub> Reduction with Ethane Oxidative Dehydrogenation by Oxygen-Modification of Molybdenum Carbide, *ACS Catal.* 8 (2018) 5374–5381. <https://doi.org/10.1021/acscatal.8b00541>.
- [31] A. Kurlov, D. Stoian, A. Baghizadeh, E. Kountoupi, E.B. Deeva, M. Willinger, P.M. Abdala, A. Fedorov, C.R. Müller, The structural evolution of Mo<sub>2</sub>C and Mo<sub>2</sub>C/SiO<sub>2</sub> under dry reforming of methane conditions: morphology and support effects, *Catal. Sci. Technol.* 12 (2022) 5620–5628. <https://doi.org/10.1039/D2CY00729K>.
- [32] Q. Bkour, C.M. Cuba-Torres, O.G. Marin-Flores, S. Tripathi, N. Ravishankar, M.G. Norton, S. Ha, Mechanistic study of the reduction of MoO<sub>2</sub> to Mo<sub>2</sub>C under methane pulse conditions, *J Mater Sci.* 53 (2018) 12816–12827. <https://doi.org/10.1007/s10853-018-2549-0>.
- [33] Y. Zheng, Y. Tang, J.R. Gallagher, J. Gao, J.T. Miller, I.E. Wachs, S.G. Podkolzin, Molybdenum Oxide, Oxycarbide, and Carbide: Controlling the Dynamic Composition, Size, and Catalytic Activity of Zeolite-Supported Nanostructures, *J. Phys. Chem. C.* 123 (2019) 22281–22292. <https://doi.org/10.1021/acs.jpcc.9b05449>.
- [34] C.G. Silva, F.B. Passos, V.T. da Silva, Influence of the support on the activity of a supported nickel-promoted molybdenum carbide catalyst for dry reforming of methane, *Journal of Catalysis.* 375 (2019) 507–518. <https://doi.org/10.1016/j.jcat.2019.05.024>.
- [35] Y. Deng, Y. Ge, M. Xu, Q. Yu, D. Xiao, S. Yao, D. Ma, Molybdenum Carbide: Controlling the Geometric and Electronic Structure of Noble Metals for the Activation of O–H and C–H Bonds, *Acc. Chem. Res.* 52 (2019) 3372–3383. <https://doi.org/10.1021/acs.accounts.9b00182>.
- [36] Z. Xie, X. Wang, X. Chen, P. Liu, J.G. Chen, General Descriptors for CO<sub>2</sub> -Assisted Selective C–H/C–C Bond Scission in Ethane, *J. Am. Chem. Soc.* 144 (2022) 4186–4195. <https://doi.org/10.1021/jacs.1c13415>.
- [37] F. Solymosi, R. Nemeth, The oxidative dehydrogenation of ethane with CO<sub>2</sub> over Mo<sub>2</sub>C/SiO<sub>2</sub> catalyst, *Cat Lett.* 62 (1999) 197–200.

- [38] J. Brenner, C.L. Marshall, L. Ellis, N. Tomczyk, J. Heising, M. Kanatzidis, Microstructural Characterization of Highly HDS-Active Co<sub>6</sub>S<sub>8</sub>-Pillared Molybdenum Sulfides, *Chem. Mater.* 10 (1998) 1244–1257. <https://doi.org/10.1021/cm970592t>.
- [39] J. Weitkamp, Catalytic Hydrocracking—Mechanisms and Versatility of the Process, *ChemCatChem.* 4 (2012) 292–306. <https://doi.org/10.1002/cctc.201100315>.
- [40] I. Sorribes, L. Liu, A. Corma, Nanolayered Co–Mo–S Catalysts for the Chemoselective Hydrogenation of Nitroarenes, *ACS Catal.* 7 (2017) 2698–2708. <https://doi.org/10.1021/acscatal.7b00170>.
- [41] X. Li, K. Qiao, F. Subhan, W. Xing, X. Liu, Z. Yan, Preparation and hydrodesulfurization properties of cobalt–molybdenum–phosphorous catalysts for removal of dibenzothiophene, *Appl Petrochem Res.* 5 (2015) 405–411. <https://doi.org/10.1007/s13203-015-0124-z>.
- [42] G. Wang, X. Zhu, J. Zhang, Y. Sun, C. Li, H. Shan, Catalytic dehydrogenation of isobutane over Co-based catalysts, *RSC Adv.* 4 (2014) 57071–57082. <https://doi.org/10.1039/C4RA08849B>.
- [43] X. Li, A.-E. Surkus, J. Rabeah, M. Anwar, S. Dastagir, H. Junge, A. Brückner, M. Beller, Cobalt Single-Atom Catalysts with High Stability for Selective Dehydrogenation of Formic Acid, *Angewandte Chemie International Edition.* 59 (2020) 15849–15854. <https://doi.org/10.1002/anie.202004125>.
- [44] H. He, C. Miao, H. Guo, W. Hua, Y. Yue, Z. Gao, Ethane dehydrogenation over Co-based MOR zeolites, *React Kinet Mech Cat.* 135 (2022) 2045–2058. <https://doi.org/10.1007/s11144-022-02231-9>.
- [45] H.M. Nguyen, G.H. Pham, R. Ran, R. Vagnoni, V. Pareek, S. Liu, Dry reforming of methane over Co–Mo/Al<sub>2</sub>O<sub>3</sub> catalyst under low microwave power irradiation, *Catal. Sci. Technol.* 8 (2018) 5315–5324. <https://doi.org/10.1039/C8CY01601A>.
- [46] H. Guo, H. He, C. Miao, W. Hua, Y. Yue, Z. Gao, Ethane conversion in the presence of CO<sub>2</sub> over Co-based ZSM-5 zeolite: Co species controlling the reaction pathway, *Molecular Catalysis.* 519 (2022) 112155. <https://doi.org/10.1016/j.mcat.2022.112155>.
- [47] M.D. Porosoff, Carbon Dioxide Reduction using Supported Catalysts and Metal-Modified Carbides, Submitted in partial fulfillment of the requirements for the degree of Doctor of Philosophy in the Graduate School of Arts and Sciences, Columbia university, 2015. <https://academiccommons.columbia.edu>.
- [48] A. Rodriguez-Gomez, J.P. Holgado, A. Caballero, Cobalt Carbide Identified as Catalytic Site for the Dehydrogenation of Ethanol to Acetaldehyde, *ACS Catal.* 7 (2017) 5243–5247. <https://doi.org/10.1021/acscatal.7b01348>.
- [49] M. Akouche, J.-P. Gilson, N. Nesterenko, S. Moldovan, D. Chateigner, H.E. Siblani, D. Minoux, J.-P. Dath, V. Valtchev, Synthesis of Embryonic Zeolites with Controlled Physicochemical Properties, *Chem. Mater.* 32 (2020) 2123–2132. <https://doi.org/10.1021/acs.chemmater.9b05258>.
- [50] S.-H. Lee, M.J. Seong, C.E. Tracy, A. Mascarenhas, J.R. Pitts, S.K. Deb, Raman spectroscopic studies of electrochromic α-MoO<sub>3</sub> thin films, *Solid State Ionics.* 147 (2002) 129–133. [https://doi.org/10.1016/S0167-2738\(01\)01035-9](https://doi.org/10.1016/S0167-2738(01)01035-9).
- [51] A. Christodoulakis, E. Heracleous, A. Lemonidou, S. Boghosian, An operando Raman study of structure and reactivity of alumina-supported molybdenum oxide catalysts for the oxidative dehydrogenation of ethane, *Journal of Catalysis.* 242 (2006) 16–25. <https://doi.org/10.1016/j.jcat.2006.05.024>.
- [52] E. Dominguez Garcia, J. Chen, E. Oliviero, L. Oliviero, F. Maugé, New insight into the support effect on HDS catalysts: evidence for the role of Mo-support interaction on the MoS<sub>2</sub> slab morphology, *Applied Catalysis B: Environmental.* 260 (2020) 117975. <https://doi.org/10.1016/j.apcatb.2019.117975>.
- [53] S. Hu, C. Melton, D. Mukherjee, A facile route for the synthesis of nanostructured oxides and hydroxides of cobalt using laser ablation synthesis in solution (LASIS), *Phys. Chem. Chem. Phys.* 16 (2014) 24034–24044. <https://doi.org/10.1039/C4CP03018D>.

- [54] L. Zhu, D. Susac, M. Teo, K. Wong, P. Wong, R. Parsons, D. Bizzotto, K. Mitchell, S. Campbell, Investigation of CoS<sub>2</sub>-based thin films as model catalysts for the oxygen reduction reaction, *Journal of Catalysis*. 258 (2008) 235–242. <https://doi.org/10.1016/j.jcat.2008.06.016>.
- [55] T.D. Nguyen, W. Zheng, F.E. Celik, G. Tsilomelekis, CO<sub>2</sub>-assisted ethane oxidative dehydrogenation over MoO<sub>x</sub> catalysts supported on reducible CeO<sub>2</sub>-TiO<sub>2</sub>, *Catal. Sci. Technol.* 11 (2021) 5791–5801. <https://doi.org/10.1039/D1CY00362C>.
- [56] A. Saravanan, K. Prasad, N. Gokulakrishnan, R. Kalaivani, T. Somanathan, Efficiency of Transition Metals in Combustion Catalyst for High Yield Helical Multi-Walled Carbon Nanotubes, *Adv Sci Engng Med.* 6 (2014) 809–813. <https://doi.org/10.1166/ase.2014.1569>.
- [57] R. Atchudan, A. Pandurangan, J. Joo, Effects of Nanofillers on the Thermo-Mechanical Properties and Chemical Resistivity of Epoxy Nanocomposites, *J Nanosci Nanotechnol.* 15 (2015) 4255–4267. <https://doi.org/10.1166/jnn.2015.9706>.
- [58] R. Atchudan, A. Pandurangan, The use of bimetallic MCM-41 mesoporous catalysts for the synthesis of MWCNTs by chemical vapor deposition, *J Mol Catal A Chem.* 355 (2012) 75–84. <https://doi.org/10.1016/j.molcata.2011.11.028>.
- [59] A.N. Christensen, H. Kvande, P.G. Wahlbeck, E. Näsäkkälä, A Neutron Diffraction Investigation on a Crystal of alpha-Mo<sub>2</sub>C., *Acta Chem. Scand.* 31a (1977) 509–511. <https://doi.org/10.3891/acta.chem.scand.31a-0509>.
- [60] T. Leisegang, A.A. Levin, J. Walter, D.C. Meyer, In situ X-ray analysis of MoO<sub>3</sub> reduction, *Cryst. Res. Technol.* 40 (2005) 95–105. <https://doi.org/10.1002/crat.200410312>.
- [61] T. Xiao, A.P.E. York, K.S. Coleman, J.B. Claridge, J. Sloan, J. Chanrock, M.L.H. Green, Effect of carburising agent on the structure of molybdenum carbides, *J. Mater. Chem.* (2001) 3094–3098. <https://doi.org/doi-org.inc.bib.cnrs.fr/10.1039/B104011C>.
- [62] S. Takenaka, T. Iguchi, E. Tanabe, H. Matsune, M. Kishida, Formation of carbon nanotubes through ethylene decomposition over supported Pt catalysts and silica-coated Pt catalysts, *Carbon.* 47 (2009) 1251–1257. <https://doi.org/10.1016/j.carbon.2008.12.051>.
- [63] E.M. Khabushev, D.V. Krasnikov, A.E. Goldt, E.O. Fedorovskaya, A.P. Tsapenko, Q. Zhang, E.I. Kauppinen, T. Kallio, A.G. Nasibulin, Joint effect of ethylene and toluene on carbon nanotube growth, *Carbon.* 189 (2022) 474–483. <https://doi.org/10.1016/j.carbon.2021.12.052>.